

A GENETIC ALGORITHM BASED MULTI-OBJECTIVE OPTIMIZATION OF SQUEALER TIP GEOMETRY IN AXIAL FLOW TURBINES: A CONSTANT TIP GAP APPROACH

H. Maral^a, C. B. Şenel^a, K. Deveci^b, E. Alpman^c, L. Kavurmacıoğlu^a, Cengiz Camci^{d*}

^a Istanbul Technical University, Department of Mechanical Engineering, 34437 Istanbul, Turkey

^b Istanbul Technical University, Energy Science & Technology Department, 34469 Istanbul, Turkey,

^c Marmara University, Mechanical Engineering Department, Göztepe Campus, 34722 Istanbul, Turkey.

^d ASME Fellow, The Pennsylvania State University, Department of Aerospace Engineering Aero-Heat Lab., University Park, PA, USA.

*Corresponding author.

Keywords: Multi-objective optimization; artificial neural networks; genetic algorithm; tip leakage flow; squealer tip; axial turbine

ABSTRACT

Tip clearance is a crucial aspect of turbomachines in terms of aerodynamic and thermal performance. A gap between the blade tip surface and the stationary casing must be maintained to allow the relative motion of the blade. The leakage flow through the tip gap measurably reduces turbine performance and causes high thermal loads near the blade tip region. Several studies focused on the tip leakage flow to clarify the flow-physics in the past. The "squealer" design is one of the most common designs to weaken to adverse effects of tip leakage flow. In this paper, a genetic-algorithm-based optimization approach was applied to the conventional squealer tip design to enhance aerothermal performance. A multi-objective optimization method integrated with a meta-model was utilized to determine the optimum squealer geometry. Squealer height and width represent the design parameters which are aimed to be optimized. The objective functions for the genetic-algorithm-based optimization are the total pressure loss coefficient and Nusselt number calculated over the blade tip surface. The initial database is then enlarged iteratively using a coarse-to-fine approach to improve the prediction capability of the meta-models used. The procedure ends once the prediction errors are smaller than a prescribed level. The present study indicates that squealer height and width have complex effects on the aerothermal performance, and optimization study allows to determine the optimum squealer dimensions.

1. INTRODUCTION

The presence of the inherent tip gap is a non-negligible source of aerodynamic loss in axial turbines. The pressure-driven fluid-flow through the tip gap is complex, turbulent and rolls into a tip leakage vortex after leaving the tip gap. Previous investigations indicated that almost one third of the aerodynamic losses in an axial turbine stage was due to this highly dissipative tip leakage flow system [1]. Moreover, the mechanical work extracted from a turbine decreases since the tip leakage flow is not turned as much as the main passage flow [2-5]. The tip leakage flow is also responsible for excessive thermal loads which may easily cause failures near blade tip region [1, 2, 6].

Several attempts were made to clarify the physics of tip leakage flow and reduce the adverse effects of it. Novel blade tip designs are frequently attempted for effective mitigation of tip leakage flows. A potential-flow based analytical model was proposed by Moore and Tilton [8] based on the experimental results in a linear cascade. Bindon [9] classified total pressure loss related to the tip clearance into three basic parts which are internal gap loss, suction corner mixing loss and endwall loss and proposed streamlined blade tips to reduce aerodynamic loss. Tallman and Lakshminarayana [10] performed a numerical calculation for the effects of tip gap height and calculated a higher leakage flow rate for a larger tip clearance. Lakshminarayana [11] stated that the relative motion between the blade tip and casing decreases the tip leakage flow rate in turbines while increases in axial compressors.

Several blade tip modifications are possible to enhance the aerothermal performance of axial turbines by weakening the tip leakage flow mass flow rate. The squealer type design represents one of the most common design concepts in the turbomachinery industry. A numerical investigation by Krishnababu et al. [4] revealed that squealer blade tip designs improved the aerothermal performance of the axial turbine blade. Lee and Kim [12] experimentally confirmed the results of Krishnababu et al. about cavity squealer designs in a linear cascade arrangement. A study by Heyes et al. [3] revealed that squealer designs can reduce the total pressure loss compared to the flat tip. They remarked that the designers should focus on reducing the leakage flow rate. Ameri et al. [13] calculated reduced leakage flow rates for squealer type designs while an increase in heat transfer to the blade tip surface was calculated. Measurements by Camci et al. [14] in a rotating test rig indicated that a partial suction side squealer design had better performance than the conventional cavity squealer design. Numerical simulations in a rotating test rig by Kavurmacioglu, Dey, and Camci [15] showed that partial squealer designs could be used to reduce the aerodynamic loss. Azad et al. [2] carried out an experimental investigation on the effects of squealer tip designs and the measurements revealed that suction side squealer had superior heat transfer performance than the pressure side squealer and conventional cavity squealer. Schabowski and Hodson [5] carried out a numerical investigation on the effects of squealer and winglet designs. Results indicated that winglet design could achieve a reduction in pressure difference across the tip gap.

Maral et al. [16] numerically studied the effects of squealer tip geometry using a non-constant tip gap approach. A computational effort on the impact of squealer designs in a wide range was performed by Senel et al. [17] revealed the complex flow structures due to the different squealer dimensions. Results indicated that an increase in the squealer height and decrease in the width of the squealer tended to enhance the aerothermal performance although complex flow structures inside the cavity had substantial effects on the overall performance. Results obtained in [16] and [17] showed that a measure to decrease aerodynamic loss might lead to an increase in heat transfer at specific tip areas. Therefore, one must apply a multi-objective optimization strategy if both aerodynamic loss and tip heat transfer are aimed to be minimized simultaneously. Deveci et al. [18] performed a multi-objective optimization study on many squealer tip

geometries by changing the tip gap and squealer width. They concluded that there are many potential squealer tip geometries as candidates to increase the aerothermal performance.

The current paper presents a multi-objective optimization of a squealer tip geometry frequently implemented in axial turbines using a genetic algorithm (NSGA-II) [19] coupled with meta-models. Artificial Neural Networks (ANN) and Support Vector Machine (SVM) concepts [20] are used and compared with each other as meta-models. Total pressure loss coefficient and the Nusselt number over the blade tip surfaces are selected as objective functions which are aimed to be minimized. As Zhou and Hodson mentioned in their study [21], both the squealer height and squealer width are playing an essential role in the aerothermal performance of a turbomachine. Therefore, in this study, the optimization parameters are selected as the squealer height and the squealer width. Unlike the research in [18] where the tip gap was allowed to decrease, the tip gap height was kept constant here to find a close-to-optimum squealer design for improved aerothermal performance.

The meta-models used in this study require a database of solutions for their training. For this purpose, CFD results previously obtained by the authors of this paper [17] are used as the initial database. After the optimization step is complete, additional CFD solutions are performed for the selected optimum geometries to validate the metamodel predictions. These additional CFD solutions are then added to the database, and the optimization is performed one more time. This procedure is repeated four times in the current

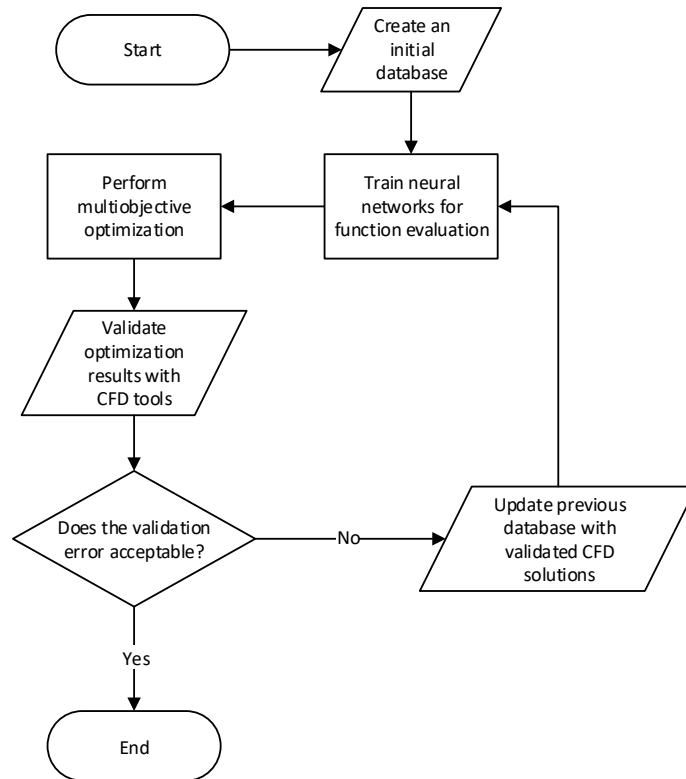


Figure 1: The work flow diagram

investigation. The computations are carried out for a single rotor blade in a linear cascade arrangement. Blade model was extracted from the 3-D rotor blade tip profile of Axial Flow Turbine Research Facility (AFTRF). The details of the aerodynamic blade tip profile from the AFTRF at Penn State University are given by Turgut and Camci [22] .

2. METHODOLOGY

The present study follows a multi-objective optimization strategy to produce a set of optimized squealer geometries for the tip leakage problem. Since a large number of experimental investigations of tip leakage flows are expensive and time-consuming in a parametric approach, a computational solution of the 3D, incompressible and steady RANS equations are employed to analyze the aerothermal performance of the squealer geometries. An initially trained meta-model (ANN and SVM) is coupled with the NSGA-II algorithm [19] to reduce the computational time spent on objective function predictions. The meta-models are trained using a database constructed from the CFD solutions. Figure 1 represents the work flow diagram for the optimization process.

Defining the Objective Functions and Design Variables

For the aerothermal optimization of the squealer geometry, the squealer width (w) and squealer height (s) are selected as design variables as depicted in Figure 2. The design variables are kept constant along the blade tip with respect to position. Unlike our previous study in [18] where the tip gap was allowed to change, the gap between the blade tip and the casing was kept constant in this effort. To improve the performance of the rotor blades, a minimum total pressure loss coefficient and minimum average Nusselt number at blade

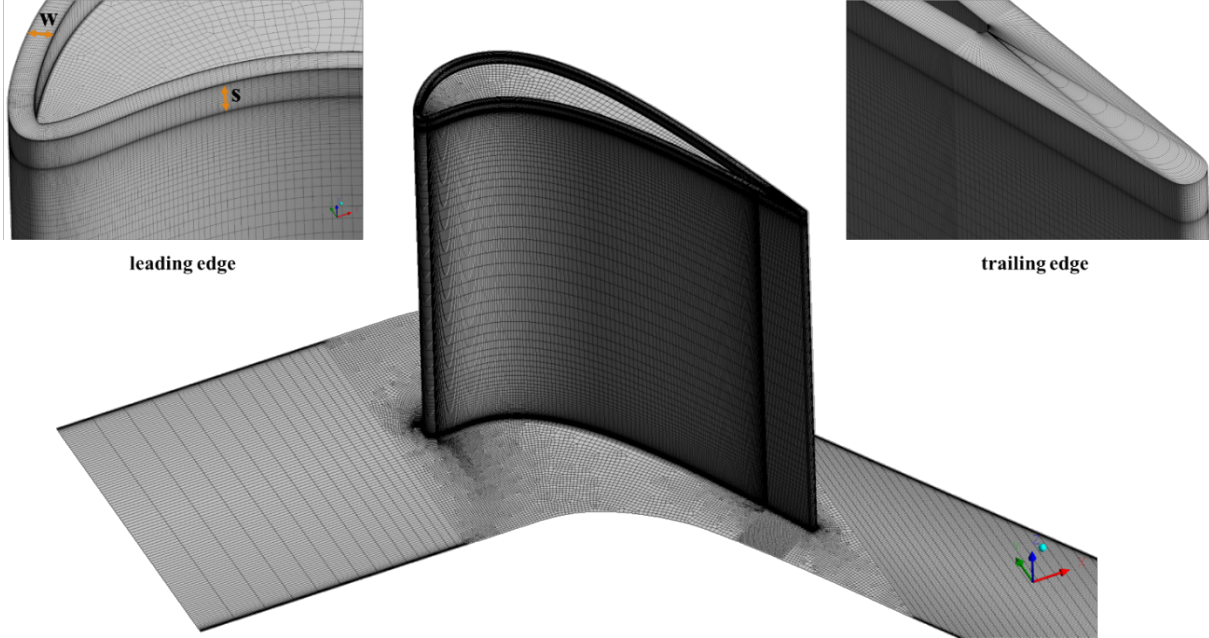


Figure 2: Design variables, width (w) and height (s) of the squealer.

tip surfaces are selected as objective functions. The total pressure loss is defined as the difference in total pressure between the inlet and exit plane of the cascade located at $0.25C_a$ distance downstream of the trailing edge. A mass-averaged total pressure at the exit plane is used.

Boundary Conditions and Solver Setup

The computations used boundary conditions from the measurements at the AFTRF test rig by Camci [23]. The numerical calculations are performed by solving the 3-D, incompressible, steady and turbulent form of the RANS equations using a finite volume method. ANSYS Fluent was used in RANS based computations. Detailed information about the boundary conditions and modeling can be found in [17].

The total pressure coefficient is as follows,

$$C_{p0} = \frac{P_0 - P_{01}}{0.5\rho U_m^2} \quad (1)$$

where P_0 is the total pressure at $0.25C_a$ distance downstream of the trailing edge, P_{01} is the mass flow averaged total pressure at the inlet and U_m (54 m/s) is the reference velocity obtained from the AFTRF test rig. The tip clearance of the blade, τ/h is equal to 1.0 % for all cases. The mass-averaged total pressure loss coefficient is calculated as follows,

$$\Delta C_{p0} = \frac{\iint \rho u C_{p0} dydz}{\iint \rho u dydz} \quad (2)$$

Thermal performance of squealer tips is compared using an average Nusselt number, \overline{Nu} ,

$$\overline{Nu} = \frac{\overline{h} C_x}{k} \quad (3)$$

where \overline{h} is average heat transfer coefficient over the tip surface and k is the thermal conductivity of the air. Local convective heat transfer coefficient is defined as,

$$h = \frac{q''_w}{T_w - T_{01}} \quad (4)$$

where q''_w is wall heat flux, T_w is wall temperature and T_{01} is the total temperature at the inlet section. Area averaged heat transfer coefficient \overline{h} , is as follows.

$$\overline{h} = \frac{1}{A} \int h dA \quad (5)$$

\overline{h} is area averaged over the cavity platform, top surface of the squealer rims and on the side surfaces in the cavity. The average heat transfer coefficient calculation uses mass-averaged total temperature at the inlet section as suggested by [24] and [4].

Creating an Initial Database

Since population-based multi-objective optimization algorithms like the NSGA-II require the objective functions to be calculated many times at each generation, coupling them directly to CFD codes becomes computationally expensive. Meta-models, which can perform fast predictions, are used to remedy this problem. Building a meta-model for function evaluation requires a database for training, testing and validation purposes. The choice of samples for preparing a database is significantly essential for the success

of predictions. Although this is one of the critical points for correct predictions, the optimum number of points that may correctly reflect the system's behavior cannot be known in advance. Even though it has been argued that the number of samples in a database is more important than the quality of design [25], a large number of samples may require extensive computational time to obtain. Also, if a database is not properly created, for example in ANN, it may result in over-learning and/or under-learning issues. Considering all of these reasons, researchers suggest that the coarse-to-fine approach which is termed as "sequential design" is an excellent alternative to one-shot procedures [26-28].

In this study, 28 different squealer geometries studied in [17] are chosen as the initial database. In [17] the design parameters for these geometries were obtained using a full factorial experiment design approach. Even though full-factorial designs may require high computational time for multi-parameter optimization problems [26, 29], they were selected in [17] mainly because there were only two design variables. The initial database used is given in Table 1.

Table 1: Initial database

Model	ΔC_{p0}	\overline{Nu}
CSQw0.6s1.2	0.1520	1001.7
CSQw0.6s1.8	0.1514	899
CSQw0.6s2.4	0.1522	830.4
CSQw0.6s3.0	0.1524	786.7
CSQw0.9s1.2	0.1515	985.9
CSQw0.9s1.8	0.1519	935.9
CSQw0.9s2.4	0.1538	865.6
CSQw0.9s3.0	0.1539	737.8
CSQw1.2s1.2	0.1520	1088
CSQw1.2s1.8	0.1462	986.9
CSQw1.2s2.4	0.1532	927.4
CSQw1.2s3.0	0.1525	876.5
CSQw1.5s1.2	0.1527	1109.5
CSQw1.5s1.8	0.1532	929.8
CSQw1.5s2.4	0.1521	960.3
CSQw1.5s3.0	0.1546	765.1
CSQw1.8s1.2	0.1532	1071.9
CSQw1.8s1.8	0.1501	1041.1
CSQw1.8s2.4	0.1528	988.6
CSQw1.8s3.0	0.1526	940.7
CSQw2.1s1.2	0.1482	1085.5
CSQw2.1s1.8	0.1512	1057.9
CSQw2.1s2.4	0.1470	940.8
CSQw2.1s3.0	0.1465	898
CSQw2.4s1.2	0.1535	1166.3
CSQw2.4s1.8	0.1525	1028
CSQw2.4s2.4	0.1511	1021.1
CSQw2.4s3.0	0.1520	979.6

In Table 1 CSQ, w and s stand for cavity squealer, squealer width and squealer height, respectively. The two digits following w and s give the width and the height in mm.

Training Meta-models for Function Evaluation

In this study, the ANN and SVM are employed as metamodels, and their prediction capabilities are compared to each other. The ANN used here is a feedforward neural network (multi-layer perceptron, MLP) consisting of one input layer, one hidden layer, and one output layer. Some of the successful applications of feedforward neural networks (FFNNs) to optimization problems can be found in [30-36]. The number of hidden layers is highly problem-specific and dramatically affects the success of the function predictions. But MLPs with one hidden layer can fit most of the engineering problems [37-40]. The number of neurons in the input layer is set to two which is equal to the number of design parameters. Since the scales of the objective functions displayed in the second and third columns of Table 1 differ considerably, separate networks are constructed for each objective function. Therefore, the output layer of each network contains only one neuron. The number of neurons in the hidden layer is allowed to change between 1 and 10. Here, for each of this number of neurons, the network is trained, validated and tested ten times, and the corresponding testing errors are recorded. The testing error is calculated as the root mean square of the difference between the test data and network predictions. After this procedure is completed, the network structure which yields the overall minimum testing error is saved as the meta-model to be used. During this network construction process, 75% of the database is used for training, 10% is used for validation, and 15% is used for testing purposes. All networks are trained with the Levenberg – Marquardt (LM) algorithm by using the neural network package of the open source scientific programming language GNU Octave [41].

The MATLAB/Octave library LIBSVM [20] is employed for the SVM used in this paper. The nu-SVR version, which is suitable for regression, is constructed with a radial basis function kernel. Since LIBSVM library always yields the same SVM for a given dataset, training is performed only once. After the meta-models are trained, they are coupled with the multi-objective optimization code separately, and optimizations are performed twice with either ANN or SVM as the meta-model.

Optimizer

In multi-objective optimization literature, a solution is said to dominate another solution if and only if the objectives of the former are better than the latter. The solutions obtained at the end of the optimization which are not dominated by any other solution form the Pareto optimal solution set. Multi-objective evolutionary algorithms search for a Pareto optimum solution set instead of a single optimum solution searched by single objective optimization algorithms [19]. Using a population-based multi-objective optimization algorithm enables the decision maker to select a tradeoff between objective functions based on the needs. It also allows the decision maker to consider manufacturability limitations.

NSGA-II is one of the population-based state-of-the-art evolutionary algorithms [42-44]. It simulates the Darwinian evolution principle in the computer environment where the individuals of the population are evolved based on the genetic reproduction mechanisms such as crossover and mutation. It uses a non-dominated sorting technique and crowding distance method to select the fittest solutions for survival [19]. For this optimization problem, an in-house developed NSGA-II code is used. The utilized NSGA-II algorithm uses Simulated Binary Crossover and polynomial mutation for offspring reproduction. For mating selection purposes, a binary tournament method with a pool size of half the population is employed. The parameters of the optimizer are given in Table 2.

Table 2: Parameters of the NSGA-II

Population Size	100
Number of Generations	300
Mutation Rate	0.1
Crossover Rate	0.9
Mutation Index	20
Crossover Index	20
Tournament Size	5

Coarse-to-Fine Approach

In order to check the prediction capabilities of the developed meta-models and the sufficiency of the database, the candidate solutions are selected from the Pareto fronts yielded by the optimizer and CFD solutions are performed for them. The next step is to compare these CFD predictions for the fitness functions against the previously obtained meta-model predictions. These new CFD solutions are then added to the database and the optimization process is repeated with this enlarged database. This procedure is continued until a consistency was observed in the meta-model predictions. This way a sequential design strategy [26] was followed in order to come up with a suitable database to train the meta-models used for fitness function predictions.

In order to select points from the Pareto front, first the aggregate of the intersite and threshold projected distance (equation (5) in [26]) for each point on the Pareto front is calculated. Then k points which yield the top k maximum distance values were selected and CFD predictions were performed for the corresponding geometries. Although optimization process is done twice with either ANN or SVM employed for objective function predictions, both meta-models use the same database for training. Therefore, even though k points are selected from each Pareto front separately, the size of the database increases by $2k$. In this study, this procedure is repeated four times. In the first step k was taken to be three while it is taken to be two in the other steps. Therefore, in four steps a total of $(3+3) + (2+2) + (2+2) + (2+2) = 18$ points are added to the database.

3. RESULTS AND DISCUSSION

Pareto fronts obtained using ANN and SVM are examined from Figure 3, consistency can be observed in the latter at the last three steps while such behavior was not shown by the former. Due to this consistency, the final size of the database is accepted to be sufficient for SVM. No additional CFD predictions obtained for the geometries of the fifth step results are displayed in Figure 3.

Despite the consistency in the Pareto fronts yielded by the NSGA-II + SVM code, solutions on the Pareto fronts are dominated by some of the designs in the database. This domination is not a fault of the optimizing algorithm, but it is due to the prediction error of the SVM method. The objective functions of the geometries in the database are recalculated with SVM, and the results are displayed in Figure 4 along with the Pareto fronts yielded by the NSGA-II + SVM code. None of the solutions in the final Pareto front is dominated.

Table 3: Optimization steps.

Step	Squealer Model	CFD Predictions		Metamodel Predictions			Difference (%)	
		ΔC_{p0}	\overline{Nu}	Model	ΔC_{p0}	\overline{Nu}	ΔC_{p0}	\overline{Nu}
1	CSQw1.9326s2.9896	0.1459	951.4	ANN	0.1529	909.4	-4.77%	4.41%
1	CSQw2.1040s2.9895	0.1474	912.8	ANN	0.1493	932.1	-1.30%	-2.11%
1	CSQw1.7605s2.9937	0.1469	939.6	ANN	0.1529	909.6	-4.12%	3.19%
1	CSQw2.3651s2.8420	0.1517	1003.6	SVM	0.1513	955.9	0.26%	4.76%
1	CSQw2.3270s2.8653	0.1518	994.6	SVM	0.1513	952.7	0.35%	4.22%
1	CSQw1.9451s2.9829	0.1453	967.9	SVM	0.1519	920.6	-4.54%	4.89%
2	CSQw1.7384s2.3385	0.1483	987.7	ANN	0.1397	972.3	5.80%	1.56%
2	CSQw1.6862s2.3360	0.1475	938.0	ANN	0.1401	968.6	5.01%	-3.26%
2	CSQw0.7590s2.9954	0.1481	796.4	SVM	0.1529	815.1	-3.24%	-2.35%
2	CSQw1.9936s3.0000	0.1468	953.7	SVM	0.1498	939.5	-2.05%	1.49%
3	CSQw1.6278s1.2000	0.1492	1066.9	ANN	0.145	1016.9	2.79%	4.69%
3	CSQw1.8874s3.0000	0.1463	954.0	ANN	0.1464	939.8	-0.06%	1.49%
3	CSQw0.6000s2.2280	0.1516	845.7	SVM	0.1521	870.9	-0.30%	-2.98%
3	CSQw1.3538s3.0000	0.1473	893.9	SVM	0.1521	873.5	-3.28%	2.28%
4	CSQw2.1053s3.0000	0.1457	957.4	ANN	0.1465	940.5	-0.55%	1.76%
4	CSQw1.7115s2.9937	0.1458	943.5	ANN	0.1485	856.3	-1.82%	9.25%
4	CSQw0.6000s2.1036	0.1517	862.8	SVM	0.1514	878.2	0.22%	-1.78%
4	CSQw1.4106s3.0000	0.1465	907.2	SVM	0.1513	885.4	-3.30%	2.40%

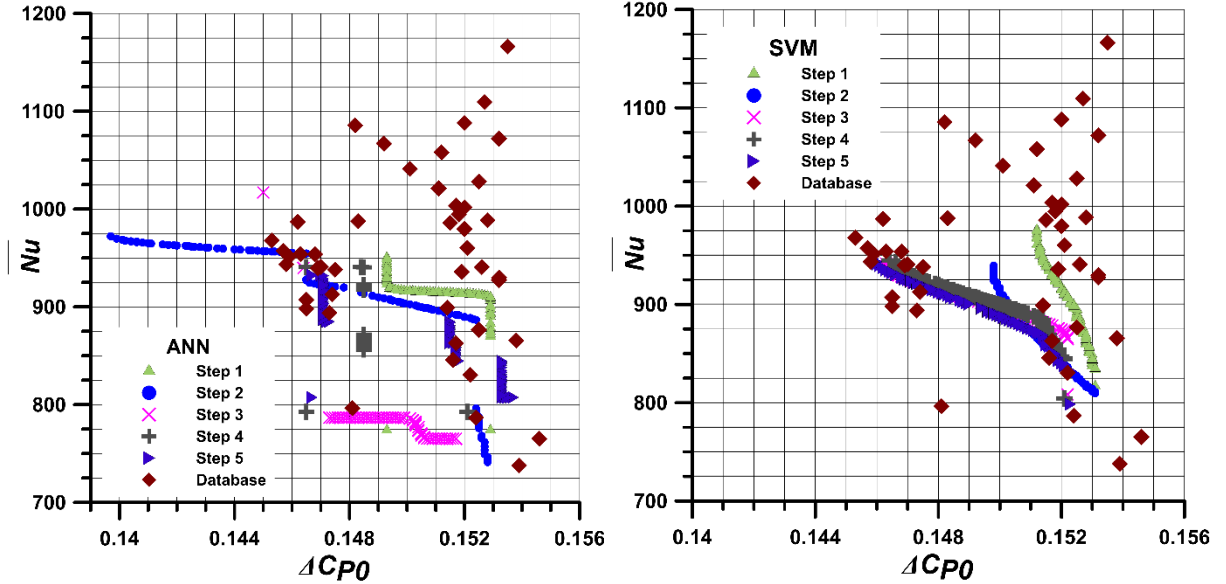


Figure 3: Pareto fronts obtained using ANN and SVM along with the database.

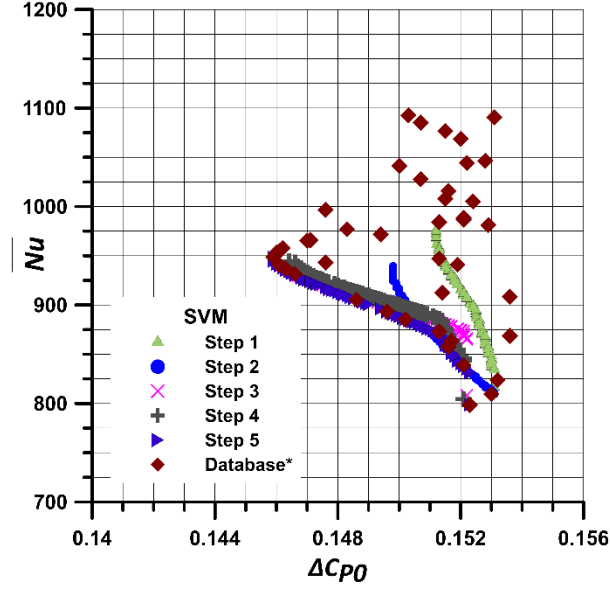


Figure 4: Pareto fronts obtained using SVM along with the database points recalculated using SVM

The objective functions of 28 geometries of the original database are given in Figure 5 along with the CFD predictions of the added geometries shown in Table 3. Figure 5 is useful to see if the optimization procedure leads to an improvement in aerothermal performance. It is clear from this figure that among the six non-dominated solutions shown in the figure, only one of them is from the original database. In addition to this, if the two objective functions are assumed to have the same importance, then the best solution is going to be the “CSQw0.7590s2.9954” followed by the “CSQw2.1s3.0” from the original database. From Table 3 and Table 1, the objective function pairs for CSQw0.7590s2.9954 and CSQw2.1s3.0 are (0.1481, 796.4) and (0.1465, 898.0), respectively. Despite the 1.09% increase in the total pressure loss, CSQw0.7590s2.9954

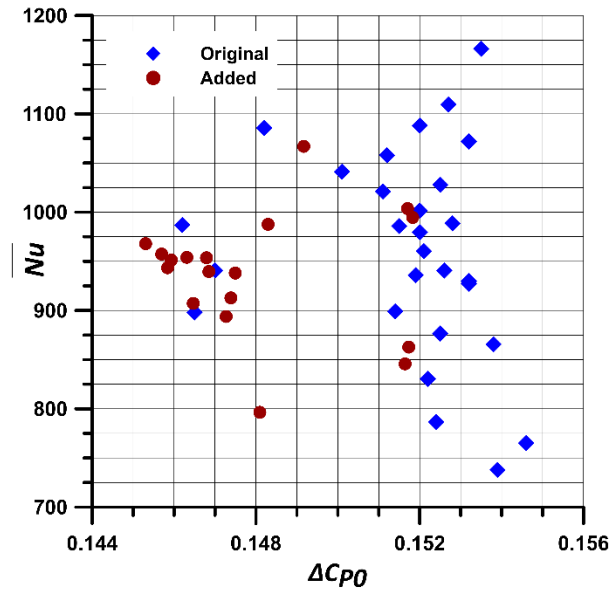


Figure 5: Objective functions of the original and optimized geometries.

provides a nearly 11% improvement in the Nusselt number. This improvement is thought to be a significant improvement. Therefore, detailed aerodynamic analyses are performed and presented for these two geometries in the next section.

Aerothermal Investigation of the Selected Geometries

This section contains detailed aerothermal investigations for CSQw0.759s2.9954 and CSQw2.1s3.0 geometries. The applied CFD methodology was previously validated by the authors in [18] for the Durham blade in a linear cascade arrangement. Except the trailing edge region, it was observed that CFD predictions were in a good agreement with the measurements[18].

The mass-averaged total pressure loss coefficient and the averaged Nusselt number normalized with respect to the flat tip are listed in Table 4. CFD results indicate both squealer designs achieve a similar reduction in total pressure loss while optimized squealer design provides a considerable reduction in averaged Nu number with respect to CSQw2.1s3.0 design. Both CSQw2.1s3.0 and CSQw0.759s2.9954 designs improved the aero-thermal performance compared to the flat tip. However, there has been much enhancement in the thermal characteristic as seen in Table 4.

Table 4: Normalized ΔC_{p0} and \overline{Nu}

Model	$\Delta C_{p0}/\Delta C_{p0,FL}(\%)$	$\overline{Nu}/\overline{Nu}_{FL}(\%)$
CSQw2.1s3.0	93.9	66.8
CSQw0.759s2.9954	94.9	59.2

Aerodynamic Investigation

Both CSQw2.1s3.0 and CSQw0.759s2.9954 squealer designs have similar aerodynamic performance. Both designs have almost the same squealer rim height while the squealer width varies in wider range. Reduction in ΔC_{p0} at exit plane is 6.1% and 5.1% respectively for CSQw2.1s3.0 and CSQw0.759s2.9954. The total pressure loss coefficient distribution at the exit plane is given in Figure 6. Loss contours reveal that location and magnitude of tip leakage vortex (LV) and passage vortex changed. LV occupies a wider region in the case of CSQw2.1s3.0 design. Core of the LV is found to be more intense in the case CSQw2.1s3.0 where the passage vortex weakens for the design selected from the initial database. Moreover, the LV comes closer to the suction side of blade for CSQw0.759s2.9954. CFD calculations indicate that optimized squealer design mitigates the tip leakage vortex compared to the CSQw2.1s3.0 design. However, a larger passage vortex is predicted for the optimized squealer design. Passage vortex spreads over a larger area and extends towards the midspan in spanwise direction. It is clearly seen that loss due to the wake is almost identical. Thus, it can be concluded that the total pressure loss due to the passage vortex dominates the reduction in the tip leakage vortex.

Leakage mass flow rates for the squealer designs are given in Table 5. A lower leakage flow rate was calculated at the gap exit for the optimized squealer design. Thus, it is expected to reduce the loss related to the tip leakage flow. ΔC_{p0} distribution at the exit plane verifies that the tip leakage vortex is weakened compared to CSQw2.1s3.0. The reduction in the leakage flow rate is due to the blockage over the suction side rim.

Figure 7 shows the loss contour plotted on axially located planes in the streamwise direction with vectors on it. The main difference between the two squealer designs is the squealer width. CSQw0.759s2.9954 has

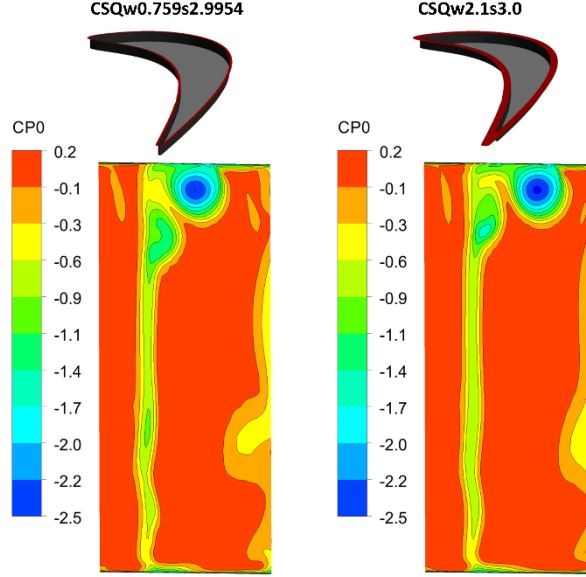


Figure 6: ΔC_{p0} distribution at exit plane.

Table 5: Leakage flow rates at the gap exit.

Model	\dot{m}_L [g/s]
CSQw2.1s3.0	7.96
CSQw0.759s2.9954	7.69

a narrower squealer rim than CSQw2.1s3.0 design. Thus, CSQw0.759s2.9954 has a larger cavity area. Therefore, a more sizeable cavity vortex is predicted inside the cavity for the optimized squealer design. The Larger cavity vortex results in higher total pressure loss in the tip gap. Besides, a wider recirculation region is observed inside the cavity. The recirculation region extends up to the upper surface of the squealer rim and brings an additional blockage on the leakage flow. A slightly higher blockage is predicted for CSQw0.759s2.9954 design. Therefore, a lower leakage flow rate and exit velocity were calculated for optimized squealer design.

Figure 7 indicates that the LV moves towards the suction side of the blade for the optimized squealer design. The shift in the tangential direction can reduce the leakage flow rate by exerting an additional blockage to the tip leakage flow. However, it is expected that the aerodynamic interaction between the tip leakage flow and the main passage flow to be higher for the optimized squealer design. Optimized design CSQw0.759s2.9954 reduced the total pressure loss related to the tip leakage vortex at exit plane. Nevertheless, lower overall loss is calculated for CSQw2.1s3.0. This result is due to the loss related to the enlarged passage vortex and increasing interaction between the leakage flow and the passage flow. Squealer designs play a crucial role on the interaction between the tip leakage vortex and the passage vortex.

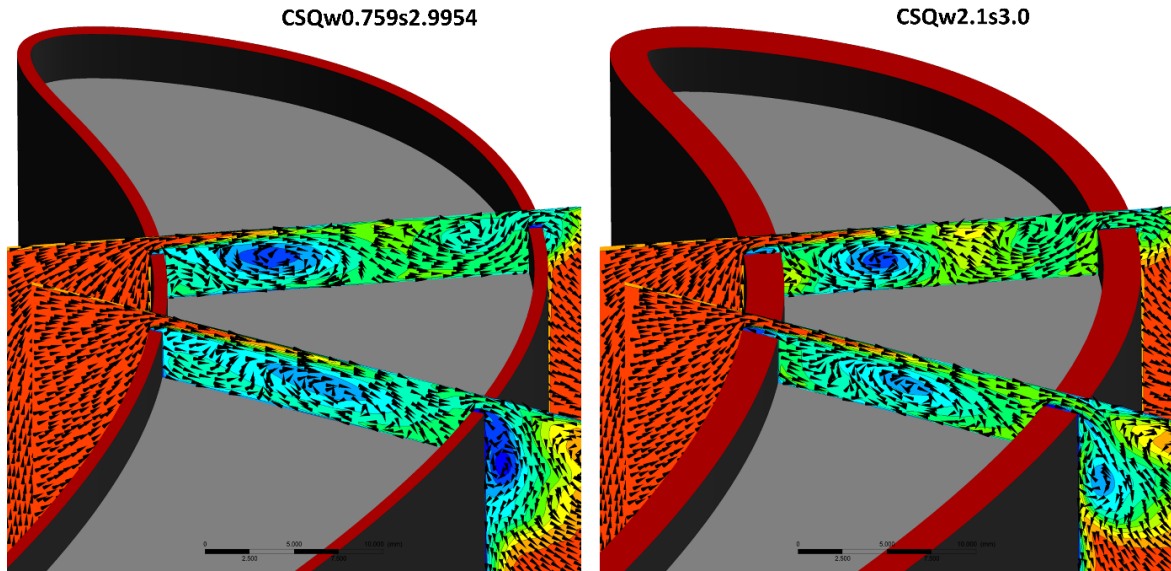


Figure 7: Loss contour and vectors on axially located planes.

Studies reveal that larger tip leakage vortex becomes dominant when compared to the passage vortex. Smaller leakage vortex in CSQw0.759s2.9954 causes larger passive vortex. The loss due to passage vortex is expected to dominate the reduction because of smaller leakage vortex in overall loss estimation.

Thermal Investigation

Both squealer designs reduced the heat load on blade tip surfaces considerably. Table 4 indicates that CSQw2.1s3.0 enabled a 33.2% reduction in averaged heat transfer coefficient while CSQw0.759s2.9954 offered a better enhancement by decreasing averaged heat transfer coefficient by 40.8%. Compared to aerodynamic performance improvement, squealer designs offer a considerable improvement in thermal performance.

Figure 8 depicts the convective heat transfer coefficients on squealer surfaces. Both squealer designs show relatively reduced the convective heat transfer coefficient near the trailing edge because of the low momentum and recirculatory cavity flow in this zone compared to the flat tip. Blue hues represent lower h areas. An elevated h zone is predicted around the leading edge because of the impingement of the incoming hot and recirculatory gas flow. The red, orange and yellow hues show the elevated heat transfer coefficients. The incoming flow passing over the squealer rim impinges on the blade tip surface in the cavity and forms a vortex pair similar to a horseshoe vortex. After impinging on the cavity surface, the leakage flow separates into two arms: one heading to the pressure side corner while the other arm moves towards the suction side rim. High thermal loads are apparent in this zone because of this flow mechanism. The CFD results reveal that squealer designs are effective in modifying high heat transfer regions. High heat transfer region extends further in the axial direction for CSQw2.1s3.0 design. The leakage flow leaving the tip gap causes high h on the top surface of the suction side rim as shown in Figure 8. Figure 7 reveals that the leakage flow passing over the vortical structures inside the cavity re-attaches on the cavity surface. Thus, relatively higher heat transfer coefficients are apparent inside the cavity between the mid-chord and the leading edge.

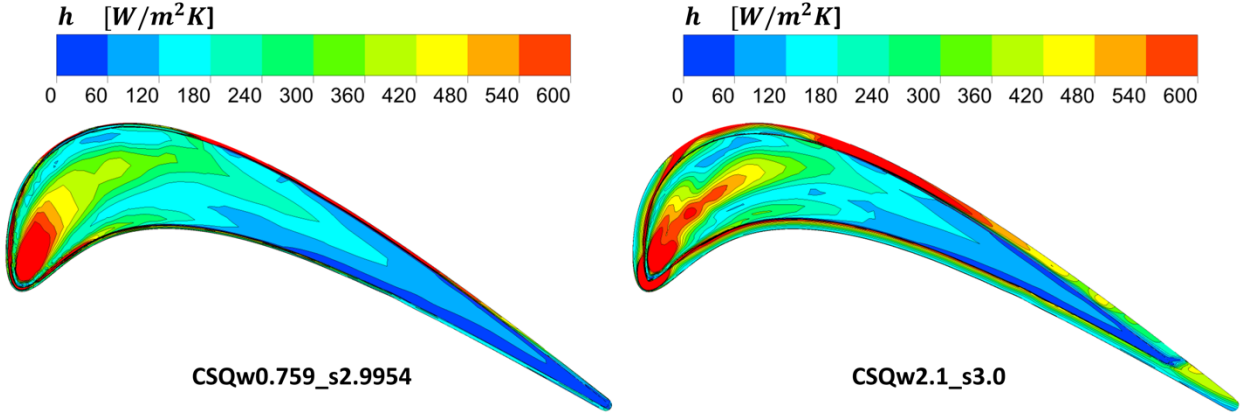


Figure 8: Averaged heat transfer coefficient distribution on squealer surfaces.

Figure 9 shows the formation of a vortex pair due to the impingement of incoming flow over the leading edge. The incoming flow impinges on the cavity surfaces and separates into two legs. One of the legs is accumulated towards the suction side corner while the remaining part is moved to the pressure side rim as seen in Figure 9. Blue and gray streamlines released from the upstream of the leading edge reveal that some of the leakage flow moves towards the camberline in the case of CSQw2.1s3.0 unlike the case

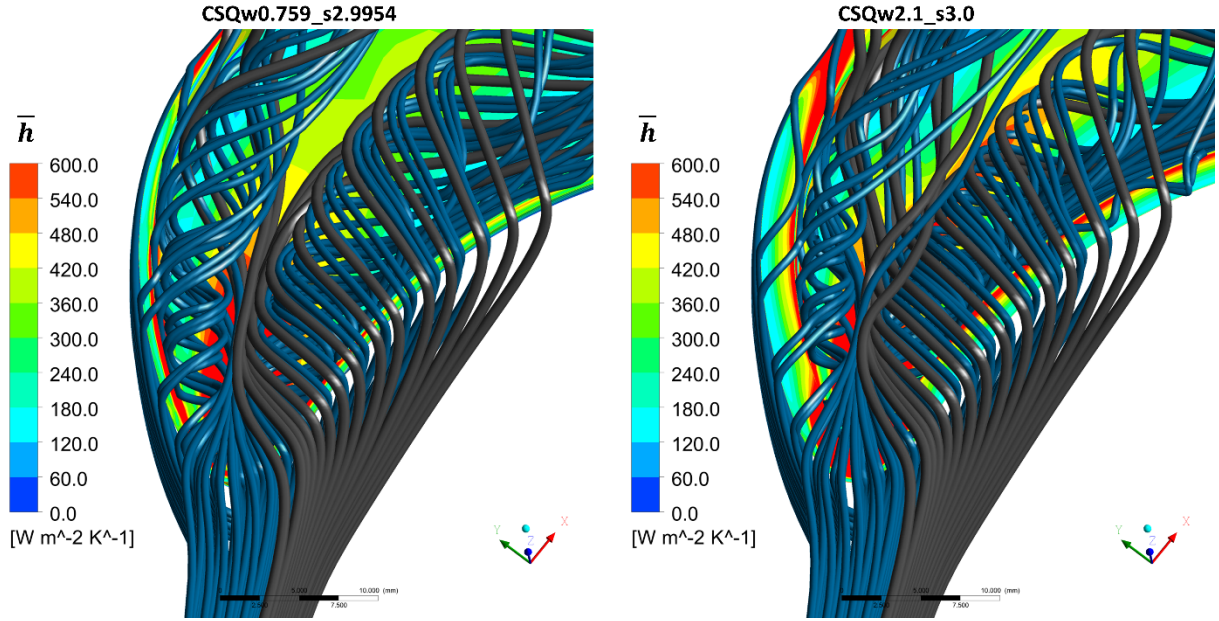


Figure 9: Formation of vortex pair which results in higher thermal loads on cavity surface.

CSQw0.759s2.9954. The streamlines moving between the suction side leg and pressure side leg is the source of the higher heat transfer to the blade tip surface. A thinner squealer rim is found to force the leakage flow to accumulate near the suction side corner and the pressure side corner. The squealer design obtained utilizing of the genetic algorithm integrated with ANN and SVM achieves a higher reduction in heat transfer when compared to CSQw2.1s3.0.

4. CONCLUSIONS

This paper deals with a multi-objective optimization technique to evaluate and compare improved squealer designs for their aerothermal characteristics. The squealer width and squealer height are the two optimization parameters and, the objective functions are area averaged Nu number and aerodynamic loss coefficient (ΔC_{p0}). The tip gap in this study is kept constant along with the blade.

The optimizer is a population-based algorithm NSGA-II coupled with a meta-model. The ANN and SVM models are tested and compared as meta-models. Since the individual CFD solutions for all of the design space are time-consuming, a course-to-fine methodology is used to explore and then exploit the design space. Therefore, the initial database is enriched with the selected solutions obtained from the Pareto fronts and meta-models are retrained for better accuracy in the predictions.

Selected results from the Pareto fronts indicate that the optimization performed in this study successfully produced designs with improved aerothermal performance. Even though the error between meta-model and CFD predictions does not drop considerably, consistency in the predictions of SVM is observed after the third step of the applied coarse-to-fine approach. Therefore, step-by-step enlarging of the database process is terminated after the fourth iteration.

Six non-dominated solutions are observed when the objective function's original database and the additions shown in Table 3 are plotted on the same figure. The optimization process found five of them. This observation shows the ability of the current multi-objective optimization procedure to improve the aerothermal performance of the squealer geometries.

The geometry having a squealer with of 0.759 mm and height of 2.9954 mm is the best squealer tip geometry when both objectives had equal importance. When the aerothermal performance of this current design is compared to the performance of the second-best design, which was the optimum of the original database; the current design provides a nearly 11% improvement in the thermal performance with only a 1.09% increase in the aerodynamic loss.

CFD results indicate that the optimized squealer design provides a considerable reduction in Nusselt number by restricting the high heat transfer near the leading edge compared to the CSQw2.1s3.0. However, CSQw2.1s3.0 design offers better aerodynamic performance than the optimized design. CSQw0.759s2.9954 reduced the total pressure loss by 5.1% compared to the flat tip whereas a reduction in the case of CSQw2.1s3.0 was equal to 6.1%.

The complex flow structures resulting from specific squealer height and width dimension strongly affect the aero-thermal performance. It is also possible that a poor selection of squealer width and height can have measurable adverse effects on aerodynamic and heat transfer characteristics as observed from the current CFD results. Optimized geometries tends to approach low ΔC_{p0} and low \overline{Nu} region, considering the objective functions values of initial and additional squealer designs., Using a genetic algorithm optimization offers a great potential to obtain improved aero-thermal performance.

In future studies, other advanced blade tip shapes will be investigated using the current optimization strategy in the rotating frame of reference of an axial flow turbine to improve the aerothermal performance..

5. ACKNOWLEDGEMENTS

The authors wish to thank to the sponsor TAI (Turkish Aerospace Industries Inc.) for the permission to publish this work. (Grant No. DKTM/2014/05) The last author Cengiz Camci also thanks to the Pennsylvania State University for its support during his sabbatical leave at Istanbul Technical University.

6. NOMENCLATURE

A	Area of the blade tip, squealer side, and cavity floor
ANN	Artificial neural network
CAD	Computer aided drawing
CFD	Computational fluid dynamics
C_{p0}	Total pressure coefficient
ΔC_{p0}	Total pressure loss coefficient
$\Delta C_{p0,FL}$	Total pressure loss coefficient for flat tip
FFNN	Feedforward neural network
h	Blade height
\bar{h}	Averaged heat transfer coefficient normalized by baseline heat transfer
k	Thermal conductivity of air
LM	Levenberg-Marquardt algorithm
MLP	Multi-layer perceptron
MSE	Mean square error
NSGA-II	Nondominated sorting genetic algorithm 2
\overline{Nu}	Average Nusselt number
\overline{Nu}_{FL}	Average Nusselt number for flat tip
P_0	Total pressure
P_{0I}	Mass flow averaged total pressure at the inlet section
q_w''	Wall heat flux
s	Squealer height
T_{0I}	Mass flow averaged total temperature at the inlet section
T_w	Wall temperature at the inlet section
τ	Tip gap height
U_m	Reference velocity obtained from AFTRF test rig $U_m = 54 \text{ m/s} = \omega.r_m$
w	Squealer width

REFERENCES

- [1] Denton, J. D. (1993). The 1993 IGTI Scholar Lecture: Loss Mechanisms in Turbomachines. *Journal of Turbomachinery*, 115(4), 621-656. doi:10.1115/1.2929299
- [2] Azad, G. S., Han, J.-C., Bunker, R. S., & Lee, C. P. (2002). Effect of Squealer Geometry Arrangement on a Gas Turbine Blade Tip Heat Transfer. *Journal of Heat Transfer*, 124(3), 452-459. doi:10.1115/1.1471523
- [3] Heyes, F. J. G., Hodson, H. P., & Dailey, G. M. (1992). The Effect of Blade Tip Geometry on the Tip Leakage Flow in Axial Turbine Cascades. *Journal of Turbomachinery*, 114(3), 643-651. doi:10.1115/1.2929188

- [4] Krishnababu, S. K., Newton, P. J., Dawes, W. N., Lock, G. D., Hodson, H. P., Hannis, J., & Whitney, C. (2008). Aerothermal Investigations of Tip Leakage Flow in Axial Flow Turbines—Part I: Effect of Tip Geometry and Tip Clearance Gap. *Journal of Turbomachinery*, 131(1), 011006-011006. doi:10.1115/1.2950068
- [5] Schabowski, Z., & Hodson, H. (2013). The Reduction of Over Tip Leakage Loss in Unshrouded Axial Turbines Using Winglets and Squealers. *Journal of Turbomachinery*, 136(4), 041001-041001-041011. doi:10.1115/1.4024677
- [6] Key, N. L., & Arts, T. (2004). Comparison of Turbine Tip Leakage Flow for Flat Tip and Squealer Tip Geometries at High-Speed Conditions. *Journal of Turbomachinery*, 128(2), 213-220. doi:10.1115/1.2162183
- [7] Mischo, B., Behr, T., & Abhari, R. S. (2008). Flow Physics and Profiling of Recessed Blade Tips: Impact on Performance and Heat Load. *Journal of Turbomachinery*, 130(2), 021008-021008. doi:10.1115/1.2775485
- [8] Moore, J., & Tilton, J. S. (1988). Tip Leakage Flow in a Linear Turbine Cascade. *Journal of Turbomachinery*, 110(1), 18-26. doi:10.1115/1.3262162
- [9] Bindon, J. P. (1989). The Measurement and Formation of Tip Clearance Loss. *Journal of Turbomachinery*, 111(3), 257-263. doi:10.1115/1.3262264
- [10] Tallman, J., & Lakshminarayana, B. (2000). Numerical Simulation of Tip Leakage Flows in Axial Flow Turbines, With Emphasis on Flow Physics: Part I—Effect of Tip Clearance Height. *Journal of Turbomachinery*, 123(2), 314-323. doi:10.1115/1.1368881
- [11] Yaras, M. I., Sjolander, S. A., & Kind, R. J. (1992). Effects of Simulated Rotation on Tip Leakage in a Planar Cascade of Turbine Blades: Part II—Downstream Flow Field and Blade Loading. *Journal of Turbomachinery*, 114(3), 660-667. doi:10.1115/1.2929190
- [12] Lee, S. W., & Kim, S. U. (2010). Tip Gap Height Effects on the Aerodynamic Performance of a Cavity Squealer Tip in a Turbine Cascade in Comparison With Plane Tip Results: Part 1—Tip Gap Flow Structure. *Experiments in Fluids*, 49(5), 1039-1051. doi:10.1007/s00348-010-0848-6
- [13] Ameri, A. A., Steinthorsson, E., & Rigby, D. L. (1998). Effect of Squealer Tip on Rotor Heat Transfer and Efficiency. *Journal of Turbomachinery*, 120(4), 753-759. doi:10.1115/1.2841786
- [14] Camci, C., Dey, D., & Kavurmacioglu, L. (2005). Aerodynamics of Tip Leakage Flows Near Partial Squealer Rims in an Axial Flow Turbine Stage. *Journal of Turbomachinery*, 127(1), 14-24. doi:10.1115/1.1791279
- [15] Kavurmacioglu, L., Dey, D., & Camci, C. (2007). Aerodynamic Character of Partial Squealer Tip Arrangements in an Axial Flow Turbine. Part II: Detailed Numerical Aerodynamic Field Visualisations via Three Dimensional Viscous Flow Simulations Around a Partial Squealer Tip. *Progress in Computational Fluid Dynamics*, 7(7), 374-386. doi:10.1504/PCFD.2007.014960
- [16] Maral, H., Senel, C. B., & Kavurmacioglu, L. (2016). A Parametric and Computational Aerothermal Investigation of Squealer Tip Geometry in an Axial Turbine: A Parametric Approach Suitable for Future Advanced Tip Carving Optimizations. (49705), V02BT38A058. doi:10.1115/GT2016-58107
- [17] Senel, C. B., Maral, H., Kavurmacioglu, L. A., & Camci, C. (2018). An Aerothermal Study of the Influence of Squealer Width and Height Near an HP Turbine Blade. *International Journal of Heat and Mass Transfer*, 120, 18-32. doi:<https://doi.org/10.1016/j.ijheatmasstransfer.2017.12.017>
- [18] Deveci, K., Maral, H., Senel, C. B., Alpman, E., Kavurmacioglu, L., & Camci, C. (2018). Aerothermal Optimization of Squealer Geometry in Axial Flow Turbines Using Genetic Algorithm. *Journal of Thermal Engineering*, 4(3), pp. 1896-1911, April, 2018, DOI:10.18186/journal-of-thermal-engineering.408701
- [19] Deb, K., Pratap, A., Agarwal, S., & Meyarivan, T. (2002). A Fast and Elitist Multi-Objective Genetic Algorithm: NSGA-II. *IEEE Transactions on Evolutionary Computation*, 6(2), 182-197. doi:10.1109/4235.996017
- [20] Chang, C.-C., & Lin, C.-J. (2011). {LIBSVM}: A Library for Support Vector Machines. *ACM Transactions on Intelligent Systems and Technology*. <https://www.csie.ntu.edu.tw/~cjlin/libsvm/>
- [21] Zhou, C., & Hodson, H. (2012). Squealer Geometry Effects on Aerothermal Performance of Tip-Leakage Flow of Cavity Tips. *Journal of Propulsion and Power*, 28(3), 556-567. doi:10.2514/1.B34254
- [22] Turgut, Ö. H., & Camci, C. (2016). Factors Influencing Computational Predictability of Aerodynamic Losses in a Turbine Nozzle Guide Vane Flow. *Journal of Fluids Engineering*, 138(5), 051103-051103-051113. doi:10.1115/1.4031879
- [23] Camci, C. (2004). A Turbine Research Facility to Study Tip Desensitization Including Cooling Flows. *VKI Lecture Series on "Turbine Blade Tip Design and Tip Clearance Treatment*, 1-26.

- [24] Ameri, A. A., & Bunker, R. S. (1999). Heat Transfer and Flow on the First-Stage Blade Tip of a Power Generation Gas Turbine: Part 2—Simulation Results. *Journal of Turbomachinery*, 122(2), 272-277. doi:10.1115/1.555444
- [25] Liu, L. (2005). Could Enough Samples be More Important than Better Designs for Computer Experiments? .Proceedings of the 38th Annual Simulation Symposium, Washington, DC: IEEE Computer Society, pp. 107–115.
- [26] Crombecq, K., Laermans, E., & Dhaene, T. (2011). Efficient Space-filling and Non-collapsing Sequential Design Strategies for Simulation-based Modeling. *European Journal of Operational Research*, 214(3), 683-696. doi:<https://doi.org/10.1016/j.ejor.2011.05.032>
- [27] Lehmensiek, R., Meyer, P., & Müller, M. (2002). Adaptive Sampling Applied to Multi-Variate, Multiple Output Rational Interpolation Models with Application to Microwave Circuits. *International Journal of RF and Microwave Computer-Aided Engineering*, 12(4), 332-340. doi:10.1002/mmce.10032
- [28] Sugiyama, M. (2006). Active Learning in Approximately Linear Regression Based on Conditional Expectation of Generalization Error *Journal of Machine Learning*, 7, 141-166.
- [29] Box, G. E. P., Hunter, J. S., & Hunter, W. G. (2005). Statistics for Experimenters: Design, Innovation, and Discovery: Hoboken, N.J. : Wiley-Interscience, c2005. 2nd ed.
- [30] Asadi, E., Silva, M. G. d., Antunes, C. H., Dias, L., & Glicksman, L. (2014). Multi-Objective Optimization for Building Retrofit: A Model Using Genetic Algorithm and Artificial Neural Network and an Application. *Energy and Buildings*, 81, 444-456. doi:<https://doi.org/10.1016/j.enbuild.2014.06.009>
- [31] Gossard, D., Lartigue, B., & Thellier, F. (2013). Multi-Objective Optimization of a Building Envelope for Thermal Performance Using Genetic Algorithms and Artificial Neural Network. *Energy and Buildings*, 67, 253-260. doi:<https://doi.org/10.1016/j.enbuild.2013.08.026>
- [32] Avcı, H., Kumlutaş, D., Özer, Ö., & Özşen, M. (2016). Optimisation of the Design Parameters of a Domestic Refrigerator Using CFD and Artificial Neural Networks. *International Journal of Refrigeration*, 67, 227-238. doi:<https://doi.org/10.1016/j.ijrefrig.2016.02.018>
- [33] Tehlah, N., Kaewpradit, P., & Mujtaba, I. M. (2016). Artificial Neural Network Based Modeling and Optimization of Refined Palm Oil Process. *Neurocomputing*, 216, 489-501. doi:<https://doi.org/10.1016/j.neucom.2016.07.050>
- [34] Magnier, L., & Haghighat, F. (2010). Multi-Objective Optimization of Building Design Using TRNSYS Simulations, Genetic Algorithm, and Artificial Neural Network. *Building and Environment*, 45(3), 739-746. doi:<https://doi.org/10.1016/j.buildenv.2009.08.016>
- [35] Tao, Y., Wang, P., Wang, J., Wu, Y., Han, Y., & Zhou, J. (2017). Combining Various Wall Materials for Encapsulation of Blueberry Anthocyanin Extracts: Optimization by Artificial Neural Network and Genetic Algorithm and a Comprehensive Analysis of Anthocyanin Powder Properties. *Powder Technology*, 311, 77-87. doi:<https://doi.org/10.1016/j.powtec.2017.01.078>
- [36] Bagheri, M., Mirbagheri, S. A., Bagheri, Z., & Kamarkhani, A. M. (2015). Modeling and Optimization of Activated Sludge Bulking for a Real Wastewater Treatment Plant Using Hybrid Artificial Neural Networks Genetic Algorithm Approach. *Process Safety and Environmental Protection*, 95, 12-25. doi:<https://doi.org/10.1016/j.psep.2015.02.008>
- [37] Rafiq, M. Y., Bugmann, G., & Easterbrook, D. J. (2001). Neural Network Design for Engineering Applications. *Computers & Structures*, 79(17), 1541-1552. doi:[https://doi.org/10.1016/S0045-7949\(01\)00039-6](https://doi.org/10.1016/S0045-7949(01)00039-6)
- [38] Hornik, K. (1991). Approximation Capabilities of Multi-Layer Feedforward Networks. *Neural Networks*, 4(2), 251-257. doi:[https://doi.org/10.1016/0893-6080\(91\)90009-T](https://doi.org/10.1016/0893-6080(91)90009-T)
- [39] Funahashi, K.-I. (1989). On the Approximate Realization of Continuous Mappings by Neural Networks. *Neural Networks*, 2(3), 183-192. doi:[https://doi.org/10.1016/0893-6080\(89\)90003-8](https://doi.org/10.1016/0893-6080(89)90003-8)
- [40] Hornik, K., Stinchcombe, M., & White, H. (1989). Multi-Layer Feedforward Networks are Universal Approximators. *Neural Networks*, 2(5), 359-366. doi:[https://doi.org/10.1016/0893-6080\(89\)90020-8](https://doi.org/10.1016/0893-6080(89)90020-8)
- [41] Retrieved from <https://www.gnu.org/software/octave/>

- [42] Datta, R., & Regis, R. G. (2016). A Surrogate-Assisted Evolution Strategy for Constrained Multi-Objective Optimization. *Expert Systems with Applications*, 57, 270-284.
doi:<https://doi.org/10.1016/j.eswa.2016.03.044>
- [43] Zhou, A., Qu, B.-Y., Li, H., Zhao, S.-Z., Suganthan, P. N., & Zhang, Q. (2011). Multi-Objective Evolutionary Algorithms: A Survey of the State of the Art. *Swarm and Evolutionary Computation*, 1(1), 32-49.
doi:<https://doi.org/10.1016/j.swevo.2011.03.001>
- [44] Lwin, K., Qu, R., & Kendall, G. (2014). A learning-guided multi-objective evolutionary algorithm for constrained portfolio optimization. *Applied Soft Computing*, 24, 757-772.
doi:<https://doi.org/10.1016/j.asoc.2014.08.026>